# SUPPLEMENTAL MATERIAL FOR:
# Spatiotemporal evolution and driving mechanisms of Cenozoic slab window volcanism in the Coast Ranges of California

**Eliel S. C. Anttila[1*], John M. Cottle[2], Demian A. Nelson[2], Ryan P. Eden[2,] and Andrew Kylander-Clark[2]**
*[1]Department of Earth Sciences, ETH Zürich, Zürich, 8092, CH*
*[2]Department of Earth Science, University of California Santa Barbara, Santa Barbara, CA, 93117, USA*
**Corresponding author: eanttila@ethz.ch*

## SUMMARY

This document contains detailed descriptions of methods for all geochronological and geochemical analyses and data reduction, a description of the integration of our geochronological and geochemical data into a paleogeographic model, three supplementary figures, and tables summarizing sample locations (Table SM1), U-Pb zircon geochronological data (Table SM2), zircon Hf isotope data (Table SM3), and a compilation of legacy geochronology of the Coast Range Volcanics (Table SM4). All supplementary material, data, and code for this work is accessible within the following GitHub repository: XXXXXX

## METHODS

*Sample preparation*

Whole rock samples of Coast Range Volcanics localities (collected between 2014 and 2024; summarized in Table SM1) were crushed in an industrial jaw crusher, and sieved to collect the resultant <500 micron grainsize fraction. This fraction was handwashed in an antiflocculant solution remove ultrafine material, and then hand-panned to isolate a heavy mineral fraction. Samples with heavy mineral fractions containing few zircon crystals were magnetically separated with a Franz device (0.4A at a 20º incline), and further separated by density in methylene iodide (MEI). Zircon crystals were individually picked from resultant heavy mineral separates, mounted in epoxy, and polished. The internal structures of the zircons were mapped with cathodoluminescence (CL) imaging using a Cameca SX-100 Electron Probe Micro-Analyzer (EPMA) with a CL detector at UC Santa Barbara.

*U-Pb zircon geochronology*

Laser ablation multi-collector inductively coupled plasma mass spectrometry (LA-ICP-MS) U-Pb geochronological analyses on zircon were completed at UC Santa Barbara, using a Cetac/Photon Machines Analyte Excite 193 nm excimer laser coupled with a Nu Plasma 3D multicollector ICP-MS, following the methods of Kylander-Clark et al. (2013). Each mounted zircon was ablated with a 20µm laser spot. The zircon *91500* (Wiedenbeck et al., 1995) was used for age calibration. Secondary zircon reference materials included *9435*, *AUSZ*, *Mudtank*, *GJ1*, and *Plesovice* (Jackson et al., 2004). *Iolite* (Paton et al., 2010) was used to correct for U-Pb mass bias and drift following the methods of Kylander-Clark et al. (2013) and Horstwood et al. (2016). The resultant U and Pb isotopic ratios were reduced according to methods outlined in Kylander-Clark et al. (2013). Dates for each analyzed grain were calculated by importing reduced U and Pb isotope ratios into *IsoplotR* (Vermeesch, 2018). Reduced ratios and all resultant dates, are tabulated in Table SM2.

For each sample, a group of zircons with young $^{206}Pb/^{238}U$ dates were identified. These analyses were used to calculate a weighted-mean age: the oldest analyses were iteratively removed until a group of zircon ages conforming to statistical standards for a single population (Wendt and Carl, 1991) was acquired. The data used to calculate these weighted mean ages are in non-italicized text in Table SM2, while analyses that did not go into the weighted mean (likely representing magmatic inheritance) are italicized. A blanket systematic uncertainty of 2%, accounting for all uncertainty criteria outlined in Horstwood et al. (2016), was then applied to the calculated weighted-mean ages for each sample. Weighted-mean ages for each sample are tabulated in Table SM1.

*Zircon Hf Isotopes*

Zircon crystals that were integrated into the weighted-mean ages calculated for each sample (e.g. those with young $^{206}Pb/^{238}U$ dates) were identified and subsequently targeted for zircon Hf isotope measurements. Zircon Hf isotopes were measured via LA-MC-ICP-MS at UC Santa Barbara, using the same Cetac/Photon Machines Analyte Excite 193 nm excimer laser coupled with a Nu Plasma 3D MC-ICP-MS used to develop U-Pb data. Laser shots, with a diameter of 40µm, were set coaxially with the 20µm pits from prior U-Pb analyses, such that the Hf isotope measurement ablation pits overlap with the U-Pb pits. Laser energy was XX, at a repetition rate of XX hz over 60-second ablation periods with a 30-second washout interval. The zircon *Plešovice* ($^{176}Hf/^{177}Hf = 0.282482 \pm 13E\text{-}06$; Sláma et al., 2008) was measured as a reference material throughout all analytical runs; *GJ1* ($^{176}Hf/^{177}Hf = 0.282000 \pm 5E\text{-}06$; Morel et al., 2008), *MUN-1* (0.282135 ± 7E-06; Fisher et al., 2011) and *MudTank* (0.282523±5.9E-05; Gain et al., 2019) served as secondary reference materials. Zircon Hf data was corrected for mass bias and reduced in Iolite (Paton et al., 2011). Across all analytical runs, corrected $^{176}Hf/^{177}Hf$ ratios of the *Plešovice* reference material yielded a mean of 0.282486.

$\varepsilon Hf_i$ values were calculated for each measured zircon relative to the chondritic uniform reservoir (CHUR; present-day $^{176}Hf/^{177}Hf = 0.282772$ and $^{176}Lu/^{177}Hf = 0.0332$; Vervoort and Blichert-Toft, 1999) using the corresponding single-grain $^{206}Pb/^{238}U$ age of the measured zircon, and a $^{176}Lu$ decay constant of $1.867 \times 10^{-11}$ $yr^{-1}$ (Söderlund et al., 2004). All zircon $^{176}Hf/^{177}Hf$ and $^{176}Lu/^{177}Hf$ ratios, as well as corresponding $^{206}Pb/^{238}U$ ages and $\varepsilon Hf_i$ values for all CRV zircon, are reported in Table SM3.

## IMPLEMENTATION OF PALEOGEOGRAPHIC RECONSTRUCTION MODEL

All CRV ages and modern locations were integrated into the paleogeographic reconstruction model of Wilson et al. (2005), which utilizes a diverse array of geological datasets and constraints to build a fault-block-based reconstruction of the development of the Pacific-North American transform margin over the past ca. 30 Myr. Model block motions and rotations have been adapted into a GPlates (https://www.gplates.org/)-compatible format; .rot and block geometry files (courtesy of D. Wilson, personal communication, 2021) used to run the model in gPlates are available in the following repository: XXXXXXXX. Each CRV locality was associated with a specific block in the reconstruction model (Table S1), typically by linking the CRV site with the block that is spatially-correlative with the modern location of the CRV locality. The syn-emplacement paleogeographic location of each CRV locality was modeled by calculating the position of each locality at the reconstruction model time equivalent to the age of the eruptive center.

There are two necessary exceptions to this workflow, both indicated with an asterix in the *PlateID* column of Table S1. The first concerns the paleogeographic reconstruction of sample IR22 (Northbrae Volcanics, Henschel et al., 2024), the present location of which is within the extent of Plate 10 in the reconstruction framework (Wilson et al., 2005). Plate 10 includes a portion of the San Francisco Bay Area found west of the Hayward Fault, but east of the San Andreas Fault; this entire region is treated as a single block throughout the duration of the reconstruction model. However, the Northbrae Volcanics (IR22) have been correlated with the Burdell Mountain Volcanics (BM22), implying dextral offset within Plate 10 of ca. 40 km. Furthermore, it remains unclear whether the paleo-Hayward fault was located west or east of the current location of the Northbrae Volcanics, introducing uncertainty into the magnitude of offset of IR22 relative to the total displacement of Plate 10. We adopt the paleogeographically-restored location of the Burdell Mountain Volcanics, tied to the motion of Plate 10, ca. 11 Ma as the emplacement location of both BM22 and IR22; IR22 is the only locality to be manually moved (to spatiotemporally correlate with the restored location of BM22) in the reconstruction.

The second exception revolves around the WR1 locality (Wagon Road Canyon volcanics, Vedder et al., 1973), which is presently located on Plate 32 in the Wilson et al. (2005) model, just west of the "Big Bend" in the San Andreas Fault (e.g. Crowell, 1979). In the Wilson et al. (2005) model, Plate 32 is dextrally offset west of a proto-San Andreas transform fault throughout the progression of the model. However, the timing of the generation of the Big Bend remains uncertain, as is the timing of the incipience of dextral offset along faults east of Plate 32 (e.g. the present-day San Andreas fault trace). As such, we present two end-member models for the restored emplacement location of WR1. WR1a (Fig. 3, main manuscript), tied to Plate 35 (located east of the modern San Andreas Fault), minimizes dextral offset of Plate 32 along the proto-San Andreas. The reconstructed location WR1b (Fig. 3, main manuscript) shows the full potential displacement of WR1 tied to Plate 32 given dextral offset along a long-lived proto-San Andreas fault located east of Plate 32. We posit that the correct reconstructed location of WR1 lies somewhere between these two end-member locations.

Shapefiles of all localities with new U-Pb ages, and their reconstructed locations, are available in the project repository (XXXXXXXX).

## REFERENCES


Crowell, J. C. (1979). The San Andreas fault system through time. *Journal of the Geological Society*, *136*(3), 293-302.

Fisher, C. M., Hanchar, J. M., Samson, S. D., Dhuime, B., Blichert-Toft, J., Vervoort, J. D., & Lam, R. (2011). Synthetic zircon doped with hafnium and rare earth elements: A reference material for in situ hafnium isotope analysis. *Chemical Geology*, *286*(1-2), 32-47.

Gain, S. E., Gréau, Y., Henry, H., Belousova, E., Dainis, I., Griffin, W. L., & O'reilly, S. Y. (2019). Mud Tank Zircon: Long-term evaluation of a reference material for U-Pb dating, Hf-isotope analysis and trace element analysis. *Geostandards and Geoanalytical Research*, *43*(3), 339-354.

Henschel, W. G., Hodgin, E. B., Grimsich, J. L., & Swanson-Hysell, N. L. (2024). The northbrae rhyolite of Berkeley (California, USA) constrains motion of the proto-Hayward Fault. *International Geology Review*, 1-15.

Horstwood, M. S., Košler, J., Gehrels, G., Jackson, S. E., McLean, N. M., Paton, C., ... & Schoene, B. (2016). Community-derived standards for LA-ICP-MS U-(Th-) Pb geochronology–Uncertainty propagation, age interpretation and data reporting. *Geostandards and Geoanalytical Research*, *40*(3), 311-332.

Jackson, S. E., Pearson, N. J., Griffin, W. L., & Belousova, E. A. (2004). The application of laser ablation-inductively coupled plasma-mass spectrometry to in situ U–Pb zircon geochronology. *Chemical geology*, *211*(1-2), 47-69.

Kylander-Clark, A. R., Hacker, B. R., & Cottle, J. M. (2013). Laser-ablation split-stream ICP petrochronology. *Chemical Geology*, *345*, 99-112.

Morel, M. L. A., Nebel, O., Nebel-Jacobsen, Y. J., Miller, J. S., & Vroon, P. Z. (2008). Hafnium isotope characterization of the GJ-1 zircon reference material by solution and laser-ablation MC-ICPMS. *Chemical geology*, *255*(1-2), 231-235.

Pampeyan, Earl H. *Geologic map of the Palo Alto and part of the Redwood Point 7-1/2'quadrangles, San Mateo and Santa Clara Counties, California*. No. 2371. US Geological Survey, 1993.

Paton, C., Hellstrom, J., Paul, B., Woodhead, J., & Hergt, J. (2011). Iolite: Freeware for the visualisation and processing of mass spectrometric data. *Journal of Analytical Atomic Spectrometry*, *26*(12), 2508-2518.

Sláma, J., Košler, J., Condon, D. J., Crowley, J. L., Gerdes, A., Hanchar, J. M., ... & Whitehouse, M. J. (2008). Plešovice zircon—a new natural reference material for U–Pb and Hf isotopic microanalysis. *Chemical geology*, *249*(1-2), 1-35.

Söderlund, U., Patchett, P. J., Vervoort, J. D., & Isachsen, C. E. (2004). The 176Lu decay constant determined by Lu–Hf and U–Pb isotope systematics of Precambrian mafic intrusions. *Earth and Planetary Science Letters*, *219*(3-4), 311-324.

Stanley, R. G. (1987). Implications of the northwestwardly younger age of the volcanic rocks of west-central California: Alternative interpretation. *GSA Bulletin*, *98*(5), 612-614.

Vedder, J.G., Dibblee, T.W., Jr., and Brown, R.D., 1973, Geologic map of the upper Mono Creek–Pine Mountain area, California: U.S. Geological Survey Miscellaneous Geologic Investigations Map I–752, scale 1:48,000.

Vermeesch, P. (2018). IsoplotR: A free and open toolbox for geochronology. *Geoscience Frontiers*, *9*(5), 1479-1493.

Vervoort, J. D., & Blichert-Toft, J. (1999). Evolution of the depleted mantle: Hf isotope evidence from juvenile rocks through time. *Geochimica et cosmochimica acta*, *63*(3-4), 533-556.
Wendt, I., & Carl, C. (1991). The statistical distribution of the mean squared weighted deviation. *Chemical Geology: Isotope Geoscience Section*, *86*(4), 275-285.

Wakabayashi, J. (1999). Distribution of displacement on and evolution of a young transform fault system: the northern San Andreas fault system, California. *Tectonics*, *18*(6), 1245-1274.

Wiedenbeck, M. A. P. C., P. Alle, F. Y. Corfu, William L. Griffin, M. Meier, F. V. Oberli, A. von Quadt, J. C. Roddick, and W. Spiegel. "Three natural zircon standards for U-Th-Pb, Lu-Hf, trace element and REE analyses." *Geostandards newsletter* 19, no. 1 (1995): 1-23.

Wilson, D. S., McCrory, P. A., & Stanley, R. G. (2005). Implications of volcanism in coastal California for the Neogene deformation history of western North America. *Tectonics*, *24*(3).

## SUPPLEMENTAL FIGURES

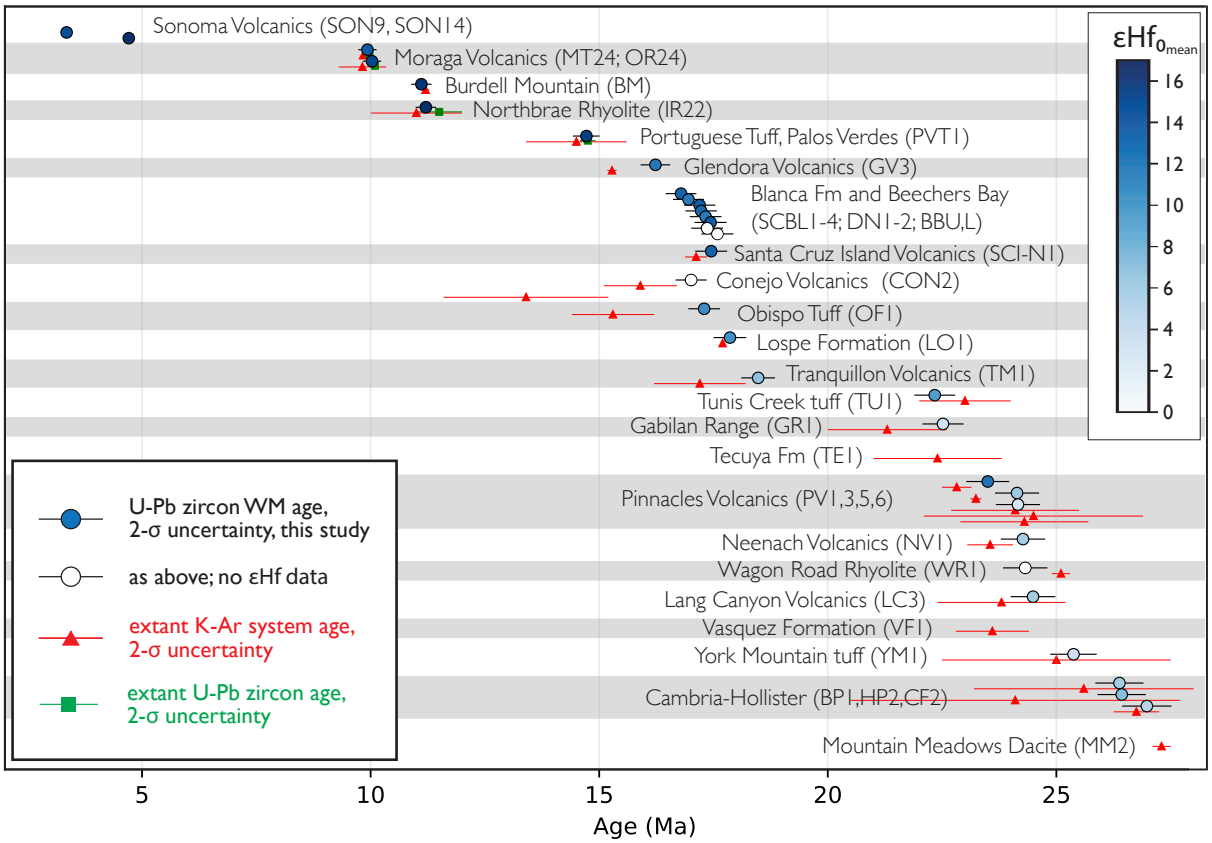


**Figure SM1:** Age and 2σ uncertainty of all localities dated with U-Pb LA-MC-ICP-MS geochronology in this study, plotted with prior K-Ar system or U-Pb zircon ages for each locality. Data and references utilized in this figure can be found here: XXXXXX

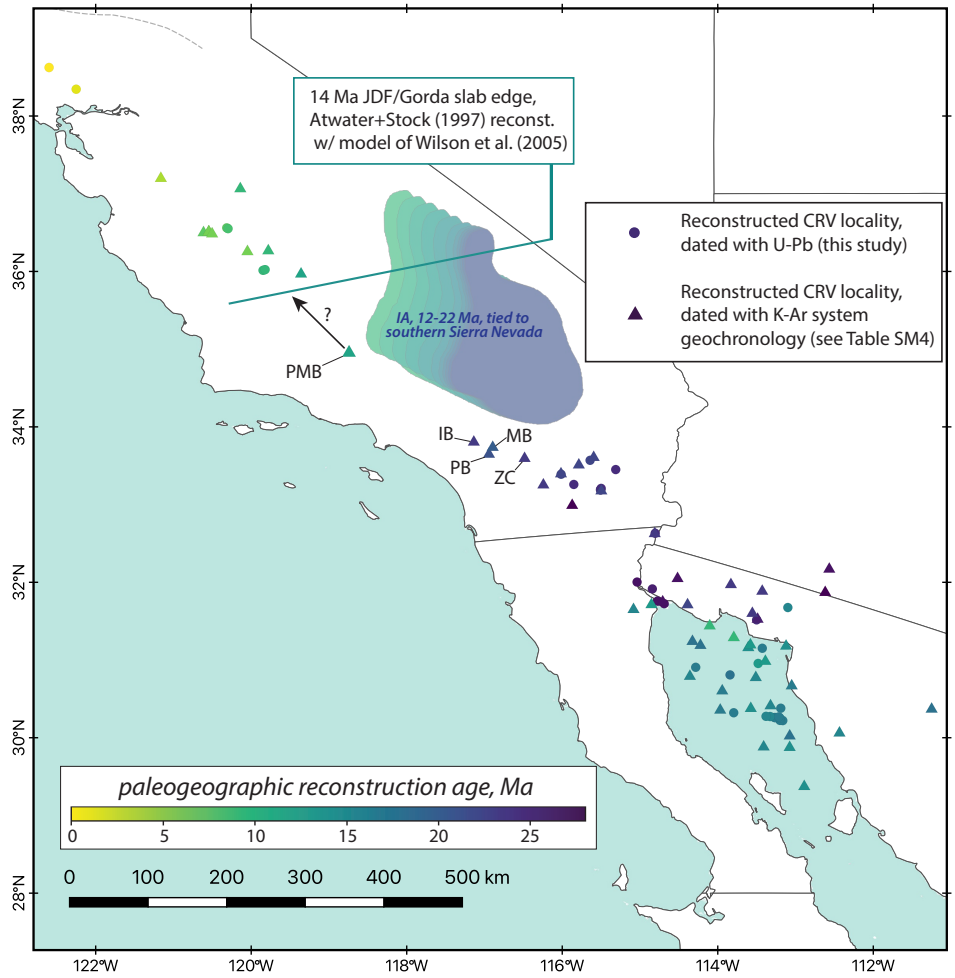


**Figure SM2:** Paleogeographically reconstructed locations of CRV localities dated with U-Pb zircon geochronology (circles, this study), and K-Ar system geochronology (triangles, references in Table SM4). Note the apparent incursion of the reconstructed emplacement locations of the Page Mill Basalt (PMB), Iversen Basalt (IB), Mindego Basalt (MB), Vaqueros intrusives (PB) and Zayante Creek intrusives (ZC) into the spatiotemporal gap in NW-trending volcanism observed in samples dated with U-Pb zircon geochronology. Analytical uncertainties on the K-Ar system ages of IB, MB, PB, and ZC all exceed 1.4 Ma (2σ; Table SM4), thus introducing significant uncertainty into the restored locations plotted in this figure. It is important to note that the incorporation of ages with large analytical uncertainties into a paleogeographic reconstruction greatly magnifies the uncertainty of the reconstructed emplacement locality. This is particularly applicable to the reconstructed locations of localities where reported radiometric analytical uncertainties do not capture broader uncertainties about emplacement/eruptive age (see discussion of the age of the Mindego Basalt in Stanley, 1987). Similarly, the Page Mill Basalt (PMB) locality has K-Ar system age control ranging from ca. 16 Ma (unpublished data of Swisher, 1999, reported in Wakabayashi, 1999) to ca. 12 Ma (Wakabayashi, 1999), with other unpublished data supporting an age of ca. 14 Ma (e.g. ages reported in Pampeyan, 1993). Analytical uncertainties of reported PMB ages allow an emplacement/eruptive age of ca. 12 Ma, which would move the restored location of the PMB even further to the north and minimize the apparent overlap of the PMB with the 22-12 Ma gap in NW-trending CRV activity.